Chapter 4

Terahertz Imaging Measurement

In this chapter, we will explore terahertz (THz) imaging for identifying water presence in flow channels of the proton exchange membrane (PEM) fuel cell. The chapter will begin with description of the THz generation and detection. Then we will explain our THz imaging system that includes a setup and sample preparation for a model cell. The THz-image results from two types of window, which are made from poly-methyl-methacrylate (PMMA) and silicon (Si), will be presented. Quantitative identification of water using a line scan plot will be implemented afterward. Two methods using a polarizer and a metal mesh in order to improve the THz image will be discussed at the end of the chapter.

4.1 Terahertz Generation and Detection

A number of the interest in THz science and technology has resulted in many different types of THz sources and sensors. In this section, we provide brief descriptions for THz generation and detection systems used in this thesis.

4.1.1 Terahertz Generation from Short Electron Bunches

Short electron bunches can be used to generate a broadband radiation at wavelength about or longer than the bunch length. This method was first predicted by H. Motz in 1951 [24]. If electron bunch can be compressed to less than one picosecond, extremely bright THz radiation can be obtain.

At the Plasma and Beam Physics (PBP) Research Facility, Chiang Mai University, Thailand, THz radiation is generated in the form of coherent transition radiation from of a few hundreds femtosecond electron bunches [25]. The system to produce such short electron bunches consists of a thermionic cathode RF-gun, an alpha magnet, and a linear accelerator (Linac), shown in Figure 4.1(left).

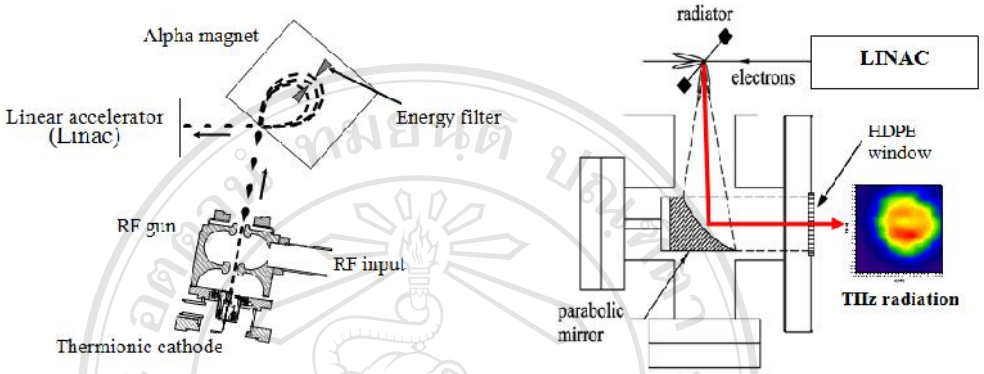

Figure 4.1: Schematic diagram of the system to generate femtosecond electron bunches (left); Schematic diagram of the THz generation system via coherent transition radiation (right).

At the THz generation station (Figure 4.1(right)), the short electron bunches from previous Linac are used to generate coherent transition radiation by passing through a radiator made of a 25.4 μm-thick Al-foil. The radiator is tilted by 45^{o} facing the electron beam direction. The backward transition radiation is emitted perpendicular to the beam axis and transmits through a high density polyethylene (HDPE) window of 1.25-mm-thick and 32-mm-diameter. The coherent radiation spectrum covering much of the far-infrared or THz spectral range and high intensity radiation from mm-waves up to 80 cm^{-1} (2.4 THz) can be detected with a room temperature pyroelectric detector.

4.1.2 Terahertz Detection

A room temperature pyroelectric device is used for detection of THz radiation intensity. The detector contains two parts: the pyroelectric sensor and the amplifier. The sensor consists of a $LiTaO_3$ pyroelectric crystal and a built-in impedance transformer which controls the overall electrical time constant of the sensor. When

the THz radiation incidents on the detector the radiation energy is converted into heat by the pyroelectric crystal [9]. A change in the crystal temperature causes the crystal to generate a polarization current. This polarization current is neutralized through an external circuit by electrodes attached to the two opposite crystal surfaces that form a capacitor. The output signal from the sensor is amplified by a signal amplifier with an adjustable gain of 1 to 200. The detector has been calibrated with a Scientech thermopile power meter [26].

4.2 Terahertz Imaging System

Preliminary measurements on non-invasive diagnostics for multilayered fuel cell structures have been conducted utilizing reflective THz imaging. The experimental setup for observing water in the PEM fuel cell is shown in Figure 4.2. The THz radiation generated from femtosecond electron bunches, as previously described, exits HDPE window port as a parallel beam. The beam is reflected off a gold-coated mirror to a THz lens of 6-cm focal-length. The THz lens focuses the beam onto a sample at approximately 30° incident angle to the normal. The beam size reduces to approximately two millimeter at the focal point where the sample is inserted. The reflected signal from the sample is collected by another THz lens of 3-cm focal-length and continued to a pyroelectric detector. The sample under investigation is placed on top of the X–Y translational stages and the THz scan using computerized motion controllers is started from top-right corner of the sample along

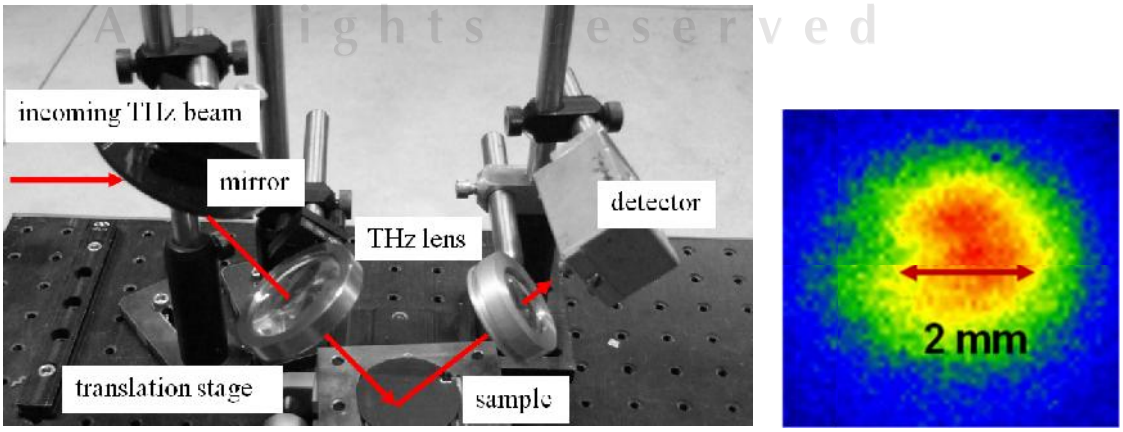

Figure 4.2: A photograph of the reflective THz imaging setup (left) and a focused beam diameter at the sample (right).

x-direction (horizontal) followed by *y*-direction (vertical) with a step of 0.5 mm throughout the experiment.

For the purpose of exploring reflective THz imaging for water identification, we prepared instead a model cell of a PEM fuel cell. Since the investigation area is in the flow channels, therefore the model cell will consist of only a flow channels plate and a window that allows THz access. We obtained a 2-mm-wide machine-through channel with a serpentine pattern from a brass plate as shown in Figure 4.3. We sealed the bottom side of the flow channel plate tightly with a cloth tape in order to ensure no liquid could escape. Then we filled some channels with water referred to as water-filled channels, while the channel left unfilled is indicated as the air-filled channel. Afterward, the window is physically placed on top of the flow channel. In this work, two types of window were investigated for image comparison. One is the PMMA window similar to the one used in the visible imaging. Another one is a Si window which is a commonly used window in THz regime. The PMMA window that we used has a thickness of 1 mm. The Si window is a silicon wafer of *p*-type doping with a thickness of 0.5 mm.

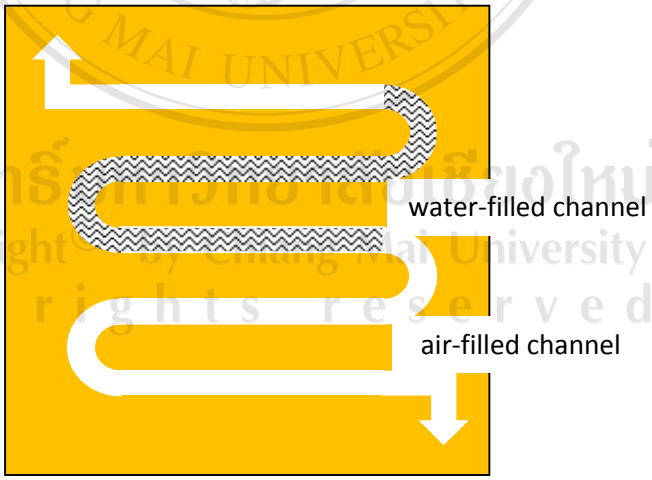

Figure 4.3: Preparation of a flow channel plate used in a model cell for THz imaging.

4.3 Reflective Terahertz Images

The ability of THz imaging for non-destructive inspection is illustrated in Figure 4.4. Figure 4.4 (a) and (b) show visible images of the model cell before and after covering with THz window, which in this case is the Si window. As can be seen, the area of flow channels is completely hidden where the window is placed. However, with our reflective THz imaging setup, we are able to obtain THz image (Figure 4.4 (c)) of the concealed region. The THz image of the flow channel region is slightly darker than that of the brass plate region which indicates differences in the reflected waveforms. Since the reflection of brass was high and that of the flow channel was low, the U shape of flow channels is recognizable.

The THz image of machine-through-brass flow channel plate with PMMA window is shown in Figure 4.5. The scanning area of 20x20 mm^2 sufficiently covers two channels: the top channel is water-filled and the bottom is air-filled. The shape of channel – even though, it seems rough around the u-bend due to a course scanning step – is still recognizable. In gray-scale, the lighter area indicates a more reflective region of brass. The darker area reveals absorptive region within the channels. Clearly, we can identify the flow channels from the image.

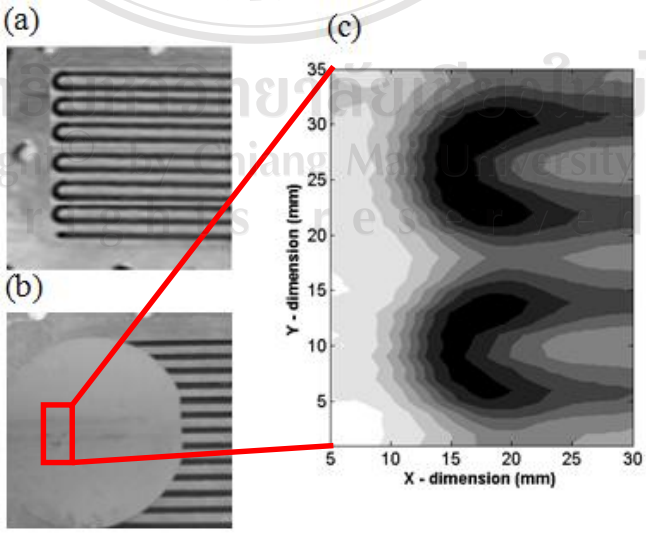

Figure 4.4: Photographs of a flow channel plate (a) before and (b) after covering with Si window; (c) THz image of (b).

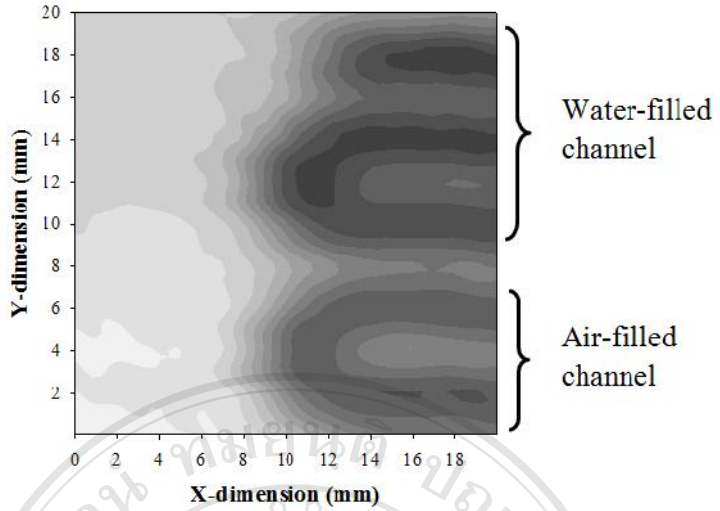

Figure 4.5: THz image of machine-through-brass flow channel plate with PMMA window.

Similarly, the THz image of machine-through-brass flow channel plate with Si window in Figure 4.6 reveals deep absorptive region in the flow channel. However, the overall reflected signals from the Si window are greater than that from the PMMA. This is because Si is more reflective and is believed to have smaller or minimal THz absorption than PMMA. Hence, the THz image using the Si window should provide more resolved image than that using the PMMA window.

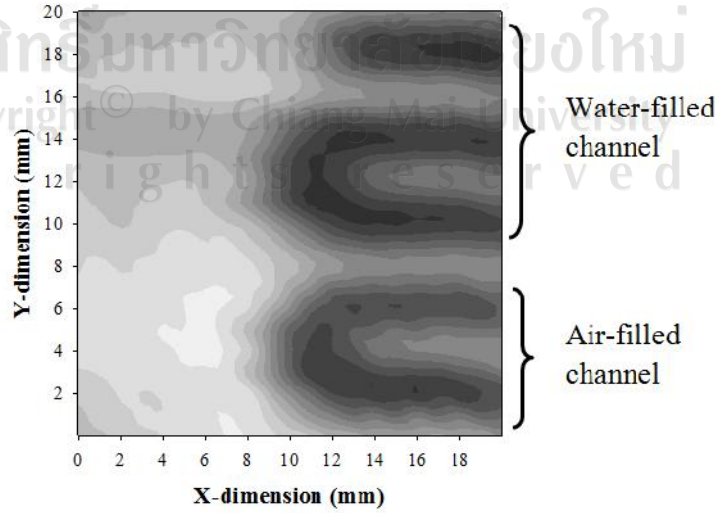

Figure 4.6: THz image of machine-through-brass flow channel plate with Si window.

4.4. Quantitative Identification of Water Presence using a Line-Scan Plot

In order to quantitatively distinguish the water-filled and the air-filled region, we perform gradient THz image and a line-scan plot shown in Figure 4.7 – 4.8. These are evident that we are able to identify water presence in the flow field with THz imaging. The gradient THz image of machine-through-brass flow channel plate with PMMA window reveals that the darker channel lies in water-filled channel as can be seen in Figure 4.7(left). Thus, we can identify the water-filled and the air-filled channels from image. In a line-scan plot (Figure 4.7(right)), this result is consistent with the reflectance of PEM fuel cell structure described in section 2.4.2, i.e., the reflected THz signal of the water area will be lower than that of the air region.

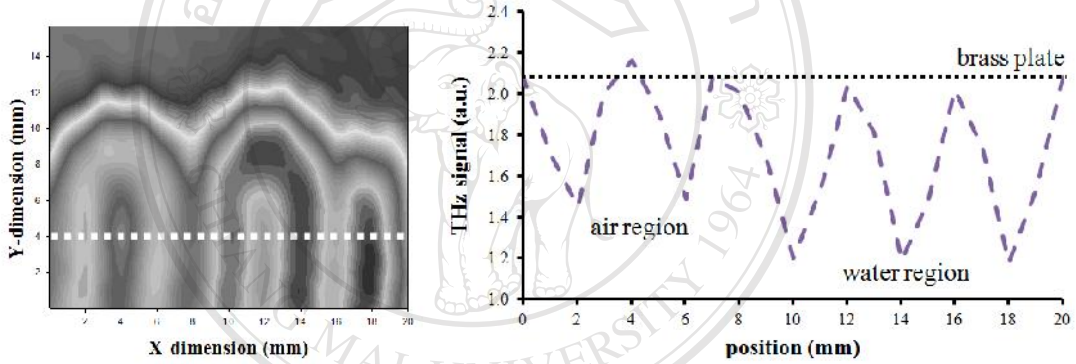

Figure 4.7: Gradient THz image with PMMA window includes the dashed line (left), and THz-signal line-scan along the dashed line in gradient THz image with PMMA window (right).

Furthermore, the gradient THz image of machine-through-brass flow channel plate with Si window in Figure 4.8(left) reveals deep absorption region in the water-filled channel. A small deeply dark area in the air-filled channel can be spotted, however, which could be attributed to the fact that our window is not tightly placed and thus there is a chance of water leakage into the air-filled channel to which THz radiation is very sensitive.

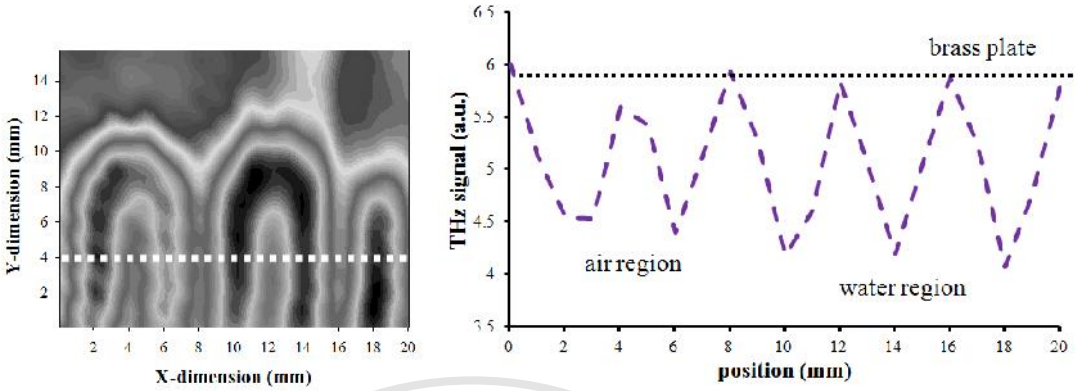

Figure 4.8: Gradient THz image with Si window includes the dashed line (left), and THz-signal line-scan along the dashed line in gradient THz image with Silicon window (right).

We will apply the line-scan plot across an arc of the flow channel to our image results, which the edge of flow channel provides strong contrast against the dielectric substrate, and use the distance between 10%-90% of signal difference from adjacent regions to define the resolution of the image (see Figure 4.9). The lesser the distance implies the better ability to distinguish two differ region, and as a result refers to the better resolution.

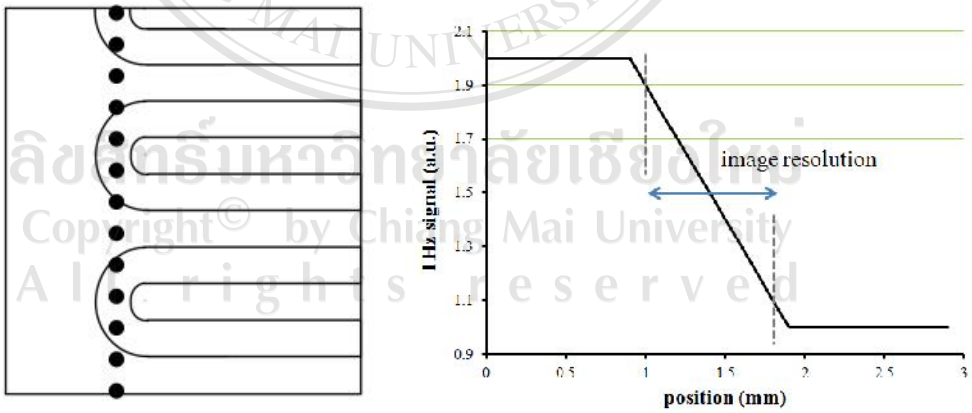

Figure 4.9: Diagram of the flow channel plate with spot of THz radiation across an arc of the flow channel (left), and using a line scan profile of region in left to define a resolution of the image (right).

4.5 Improvement of Image Resolution

The resolution is generally the key to determine the quality of the image. In this section, we discuss the spatial resolution in the context of the geometrical configuration of the reflective THz imaging system. In prior work, reflective THz imaging is excellent tool in identifying water region, air region and shape of flow channel. However, it is generally not sufficient to identify edge of flow channel. In this section, we insert a linear polarizer or a metal mesh filter into the existing setup in an effort to improve spatial resolution of THz image.

4.5.1 Using a Polarizer

Free-standing metal-wire grids are commonly used as a polarizer in the THz region. Figure 4.10(a) shows a wire grid polarizer from Graseby-Spec (Model IGP223) used in our experimental setup. The polarizer consists of 4-μm wire grid photo-lithed onto a polyethylene substrate. Figure 4.10(b) shows the insertion of the polarizer to our reflective THz imaging setup. There are two types of polarizations: the p-polarization, also known as parallel polarization or π-polarization, which the electric fields lie on the plane of incidence; and the s-polarization, also known as perpendicular polarization or σ-polarization, which the electric fields are perpendicular to the plane of incidence. From our setup configuration, we aligned the polarizer in p- and s- polarizations as indicated. Figure 4.11 shows the cross section of p- and s- polarization of THz radiation beam.

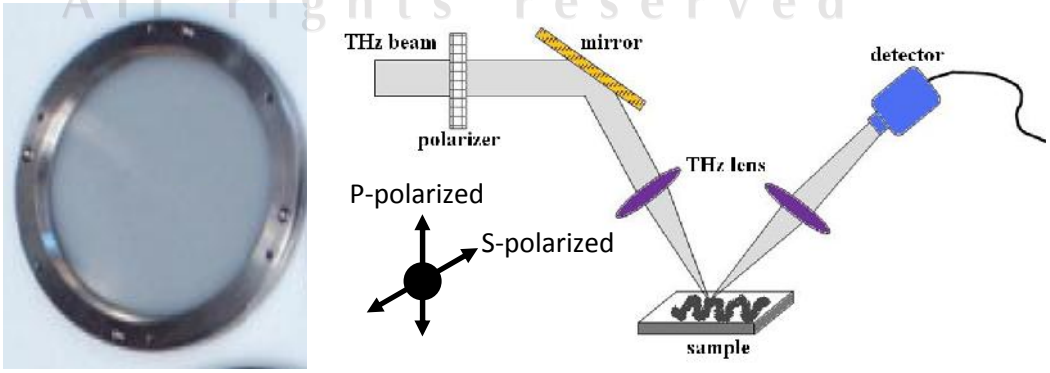

Figure 4.10: The polarizer (left); Insertion of the polarizer to our reflective THz imaging setup (right).

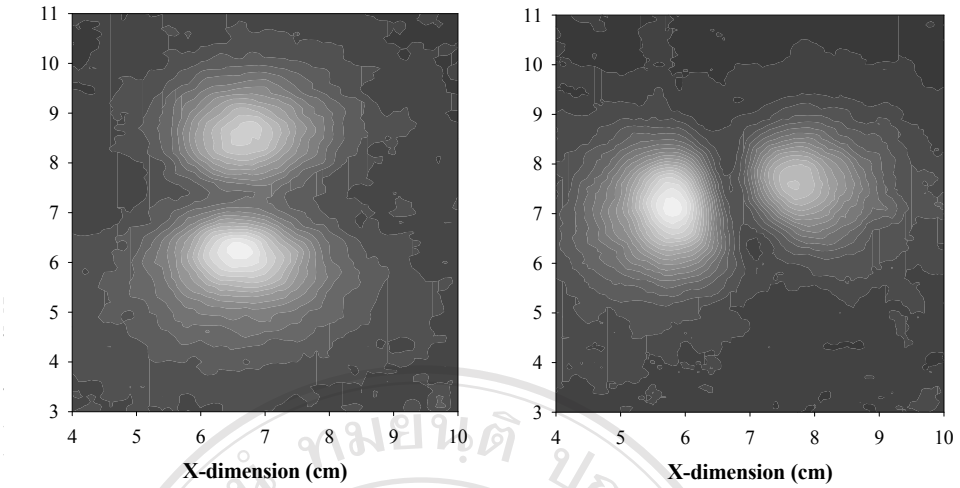

Figure 4.11: P-polarization (left) and S-polarization (right) of THz radiation beam.

In Chapter 2, the reflectance spectrum of THz radiation from normal incidence is described. For oblique incidence, particularly for 30º incidence, the formalism of transfer matrices and reflective index for normal incidence translates almost verbatim to the case of oblique incidence. By separating the THz radiation into transverse and longitudinal components with respect to the direction of the layer was constructed, we found that the transverse components are identical to transfer matrix relationships as in the case of normal incidence, provided that we replace the media refractive index n by the transverse refractive index n_T defined below and add term $cos\theta$ to the phase thickness, i.e.,

$$n_T = \begin{cases} \frac{n}{cos\theta}, & p-polarization \\ ncos\theta, & s-polarization \end{cases} \tag{4.1}$$

Figure 4.12 illustrates reflectance THz spectra of PEM fuel cell structure type air|Si|air for both types of polarizations. The graphs show the nonpolarization, p-polarization and s-polarization reflectance $|\Gamma_T(f)|^2$ as functions of frequency for the angle of incidence $\theta = 30°$. We can state that peak to peak of nonpolarization, p-polarization and s-polarization reflectances are 70%, 64% and 77%, respectively. Different of maximum peak between p-polarization and s-polarization reflectance is about 13%. The s-polarization of THz radiation yields higher reflectance response than the p-polarization.

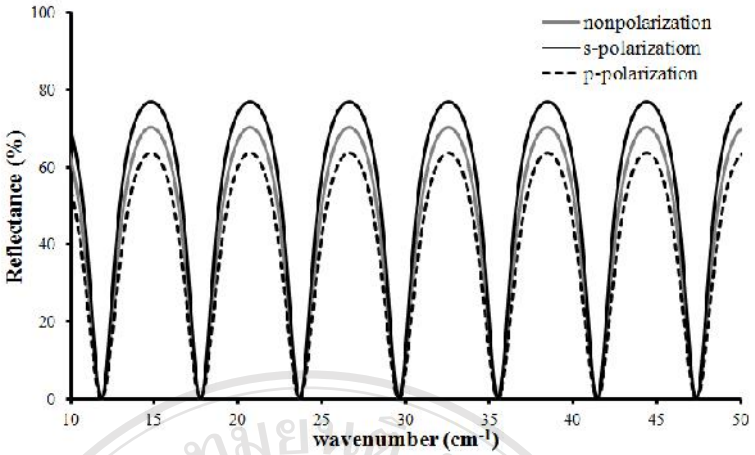

Figure 4.12: Reflectance spectra of the air|Si|air structure at 30 degree incident angle as a function of polarization.

In Figure 4.13 and 4.14, the effect of polarized THz radiation on the reconstructed image of the model cell is illustrated. The overall reflected signals from the s-polarization are greater than that from the p- polarization, as predicted by the calculation. The u-shape of the channel in the s-polarized THz image is more recognizable than that in the p-polarized THz image.

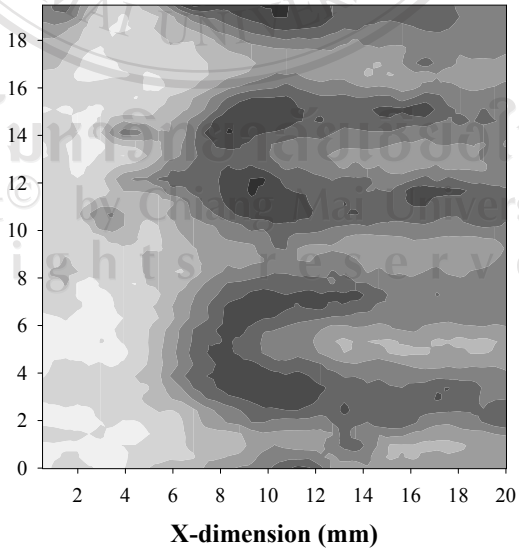

Figure 4.13: THz image using p-polarized THz radiation.

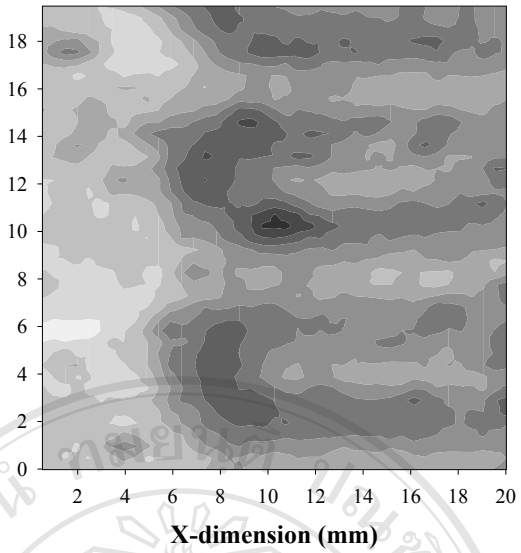

Figure 4.14: THz image using s-polarized THz radiation.

Quantitative analysis for image resolution using a line scan plot is shown in Figure 4.15. The scans compare ideal profiles at the arc of the cell with the profiles obtained from p-polarized and s-polarized THz images. Under the current setup with 30 degree of incident angle, the distance between the 90% and the 10% of maximum signal level is 2.3 ± 0.5 mm for p-polarization, while it is 2.2 ± 0.5 mm for the s-polarization. This result has ended inconclusive that the spatial resolution for s-polarization is better than that for p- polarization, although, the calculation and the measurement conclude in the same way in favor of the s-polarization. However, increasing incident angle should improve the resolution using the polarizer.

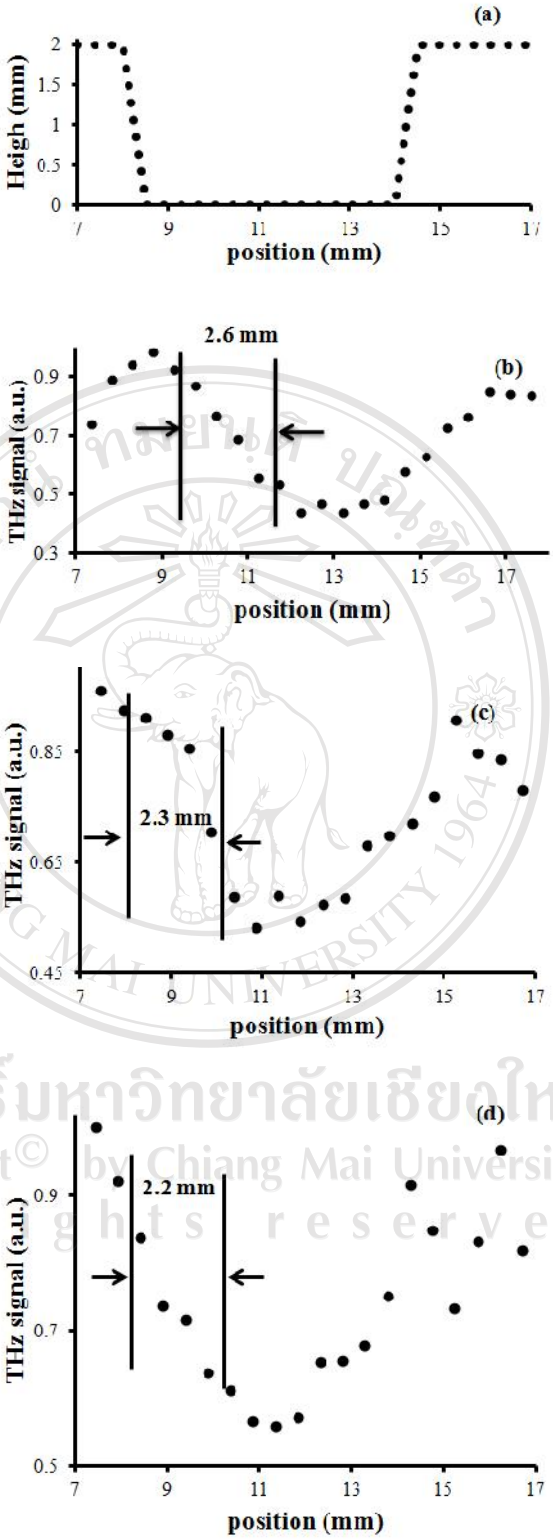

Figure 4.15: Line scans illustrate (a) real profile of the flow channel groove at the arc of the cell compared the THz signal with (b) resolution of 2.6 mm by using nonpolarized THz radiation, (c) resolution of 2.3 mm by using p-polarized THz radiation, and (d) resolution of 2.2 mm by using s-polarized THz radiation.

4.5.2 Using a Metal Mesh filter

As point out in section 2.4, a metal mesh filter is one of radio-frequency filtering methods to select frequency band in the electromagnetic waves. To confirm these transmissions spectra with the calculation provided in section 2.4, we measure the power spectrum which passes through the mesh filter. A Michelson interferometer was used to analyze the radiation spectral distribution of THz after mesh filtering. A schematic diagram of a THz Michelson interferometer is shown in Figure 4.16. The interferometer consists of a beam splitter, a fixed mirror and a movable mirror, arranging as the diagram shown. Radiation after passing through the metal mesh enters the Michelson interferometer. Then it is split into two parts by the beam splitter. The two parts next travel in two different directions to be reflected back by mirrors. After that, the two radiation pulses are combined again and sent to a detector for measuring the intensity which is called the interferogram. The radiation power spectrum is obtained after fourier transform the interferogram with the help of MATLAB programming.

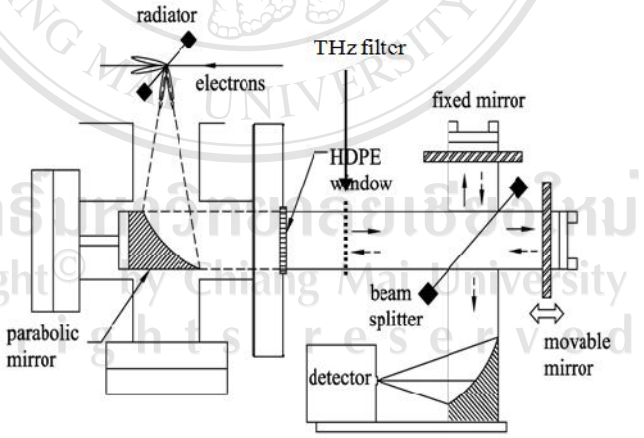

Figure 4.16: Measurement of THz power spectrum after mesh filtering via Michelson interferometer.

The transmission spectra of THz radiation without and with mesh filtering are shown in Figure 4.17. We compare transmission bands at full width half maximum of three different mesh filters as listed in Table 4.1. The measured transmission band of each mesh filter is close to the calculated one. As the mesh number increased, the

transmission band is shifted towards high frequency components. According to Rayleigh criterion (see details in appendix A), the focused beam size will become smaller for higher frequency radiation source. In other words, the mesh-80 will provide the smallest focused beam size comparing to the other two mesh filters.

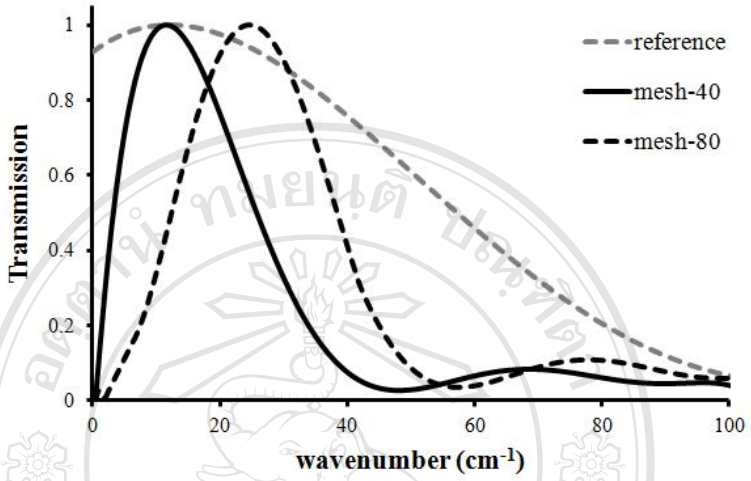

Figure 4.17: Transmission spectra of THz radiation obtain from measurement Michelson interferometer.

Table 4.1: Transmission wavenumber of THz radiation obtain from mesh filter.

Mesh	descriptions	Transmission wavenumber (cm^{-1})	
		Theory	measurement
Mesh-40	Opening size 380 μm Wire diameter 254 μm	10 – 22	5 – 25
Mesh-80	Opening size 180 μm Wire diameter 139.7 μm	18 – 54	20 – 40

Figure 4.18 is a photograph of the copper mesh filters and how we insert it in our imaging setup. We compare THz image obtained from using mesh-40 and mesh-80 as can be seen in Figure 4.19 – 4.21.

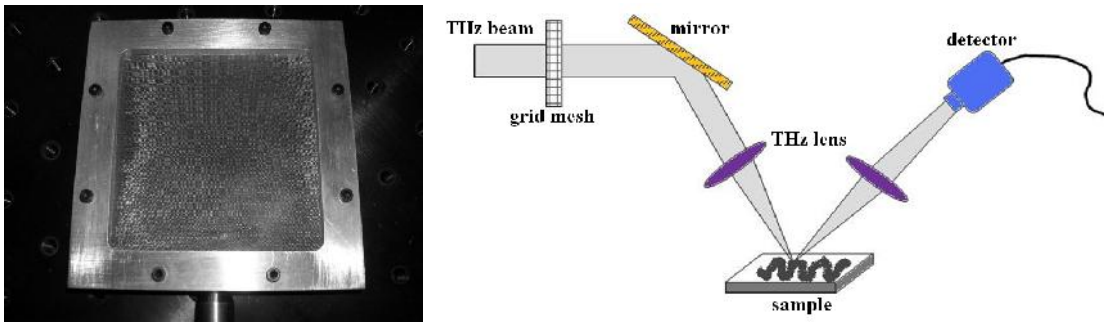

Figure 4.18: Photo of copper mesh filter with opening size 180 ×180 mm^2 (left); Reflective THz imaging system with inserting metal mesh (right).

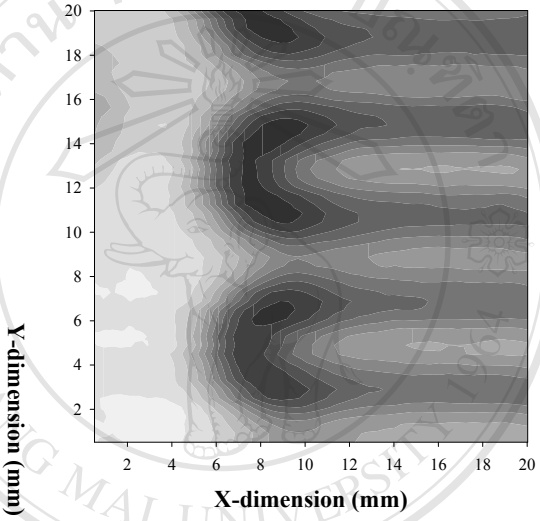

Figure 4.19: THz image of machine-through-brass flow channel plate without mesh.

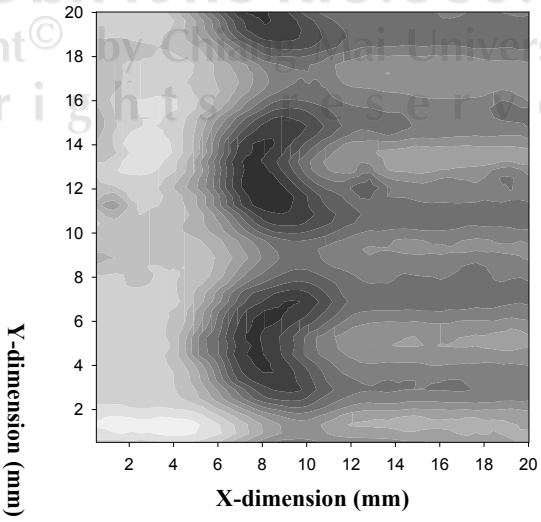

Figure 4.20: THz image of machine-through-brass flow channel plate with mesh-40.

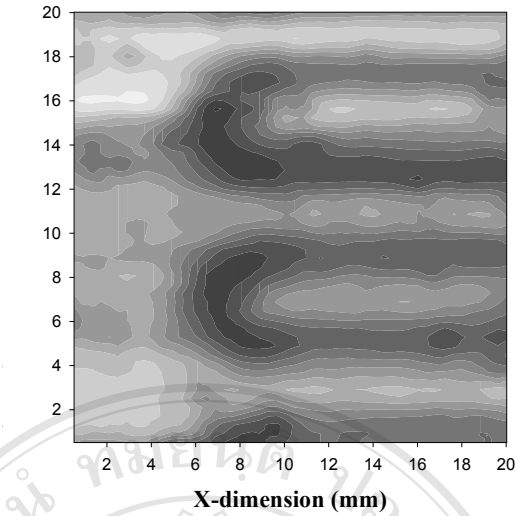

Figure 4.21: THz image of machine-through-brass flow channel plate with mesh-80.

We investigated the spatial resolution of our reflective THz imaging by performing a line-scan plot across an arc of the flow channel. The edge of flow channel provides strong contrast against the dielectric substrate. Figure 4.22(a) illustrates the real profile of an arc of the flow channel having a width of 6 mm for reference. An abrupt decrease of the THz signal is observed when the detector moves from a position over a rib of the flow channel to the trench etched into the flow channel, as shown in Figure 4.22. By using the same method in section 4.5, we found that resolution of THz image without mesh is approximately 2.6 ± 0.5 mm as can be seen in Figure 4.22(b). We can quantify the spatial resolution of reflective THz image as 1.9 ± 0.5 mm for using mesh-40, and as 1.7 ± 0.5 mm for using mesh-80. In fact, sub millimeter resolution can be improved by using a THz band-pass filter. Furthermore, higher mesh number, which in this case is mesh-80, indeed provides a better resolution.

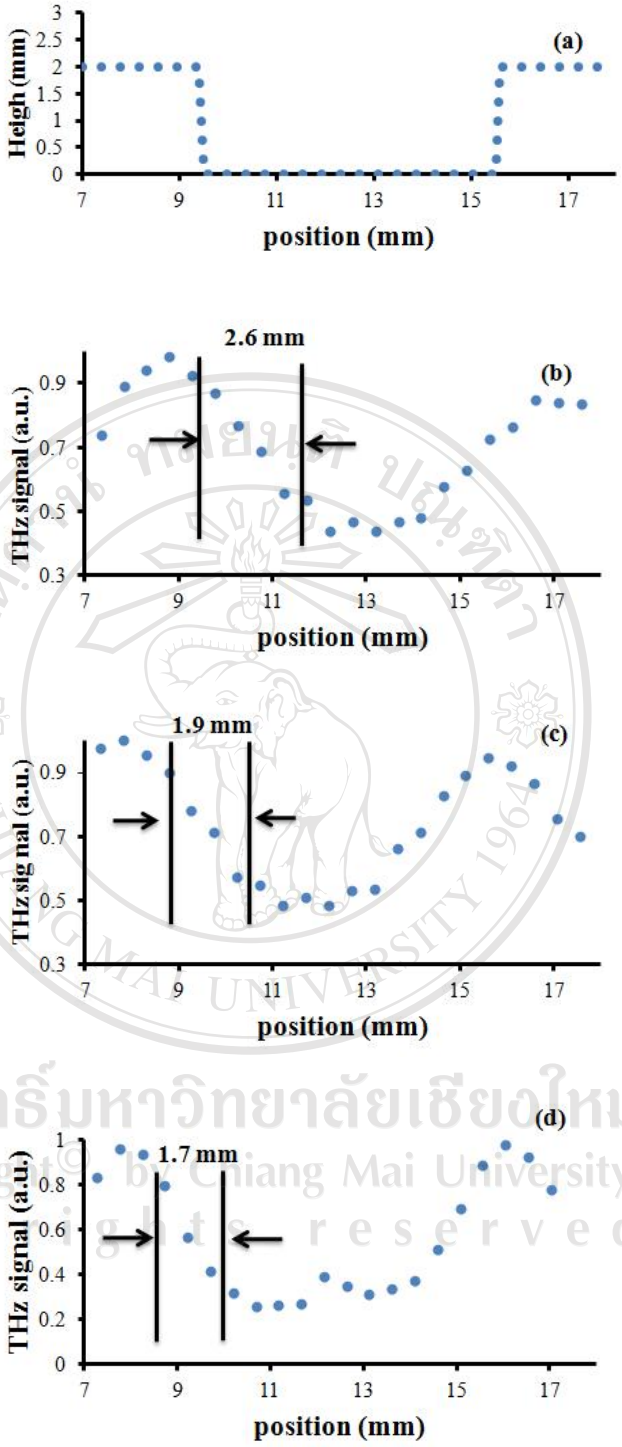

Figure 4.22: Line scans illustrate (a) real profile of the flow channel groove at the arc of the cell compared to THz signal with (b) resolution of 2.6 mm without mesh; (c) resolution of 1.9 mm with mesh-40; (d) resolution of 1.7 mm with mesh-80.

4.6 Summary

The focus of Chapter 4 was to demonstrate a possibility of THz imaging for identifying water presence in flow channels of a PEM fuel cell. The reflective THz imaging system was successfully established and the THz images were obtained from two types of THz window materials. Both PMMA and Si windows can satisfactory distinguish flow region in the machine-through-brass flow channel from the air-filled region. However, the Si window provides greater reflected signals yielding more depth into details of the image than the PMMA window.

The line-scan plot is adopted in order to quantitatively compare spatial resolution of the THz image. Under the current setup with 30 degree of incident angle, insertion of a polarizer to our THz imaging system results in image resolutions of 2.3 ± 0.5 mm and 2.2 ± 0.5 mm for p-polarized and s-polarized THz radiation, respectively. Increasing incident angle should improve the resolution using the polarizer. Using metal mesh filtering is another way to improve the image resolution. We placed a copper mesh grid wire in our THz imaging system. The calculation suggests lower frequency components will be filtered out more with higher mesh number, which results in smaller focusing beam size. Accordingly, the experiment spatial resolution of 180x180 μm^2 mesh is better than that of 380x380 μm^2 mesh. We can quantify the spatial resolution of reflective THz image as 1.9 ± 0.5 mm for using 380x380 μm^2 mesh, and as 1.7 ± 0.5 mm for using 180x180 μm^2 mesh.